CO-Induced Smoluchowski Ripening of Pt Cluster Arrays on the Graphene/Ir(111) Moiré

Timm Gerber,[†,*] Jan Knudsen,[‡,§] Peter J. Feibelman,[⊥] Elin Grånäs,[‡] Patrick Stratmann,[†] Karina Schulte,[§] Jesper N. Andersen,[‡,§] and Thomas Michely[†]

[†]II. Physikalisches Institut, Universität zu Köln, Zülpicher Str. 77, 50937 Köln, Germany, [‡]Division of Synchrotron Radiation Research and [§]MAX IV Laboratory, Lund University, Box 118, 22 100 Lund, Sweden, and [⊥]Sandia National Laboratories, Albuquerque, New Mexico 87185-1415, United States

ABSTRACT Regular Pt cluster arrays grown on the moiré template formed by graphene on Ir(111) were tested for their stability with respect to CO gas exposure. Cluster stability and adsorption-induced processes were analyzed as a function of cluster size, with *in situ* scanning tunneling microscopy and X-ray photoelectron spectroscopy. Small clusters containing fewer than 10 atoms were unstable upon CO adsorption. They sintered through Smoluchowski ripening—cluster diffusion and coalescence—rather than the frequently reported Ostwald ripening mediated by metal−adsorbate complexes. Larger clusters remained immobile upon CO adsorption but became more three-dimensional. Careful analysis of the experimental data complemented by *ab initio* density functional theory calculations provides insight into the origin of the CO-induced Pt cluster ripening and shape transformations.

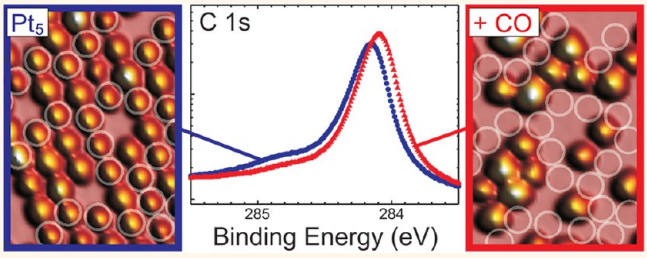

KEYWORDS: graphene · cluster · Smoluchowski ripening · sintering · carbon monoxide · diffusion · adsorption

Polydisperse metal particles randomly distributed on a porous ceramic support are widely used as industrial catalysts.[1] Their favorable behavior stems both from exceptional surface-to-volume ratios, such that a large fraction of a cluster's atoms are exposed to reactants,[2] and in certain cases also from an electronic structure modified by quantum size effects.[3] A key problem in catalyst development, accordingly, is stability at elevated temperatures and in the presence of reactants (*i.e.*, under reaction conditions). Sintering, a decrease in particle number and corresponding increase of particle size, degrades catalysts.[4−6] It is the subject of the present work.

Case studies have shed light on sintering mechanisms at the atomic level. An important one[7−15] is that under reaction conditions clusters are disrupted and form mobile metal reactant species which cause mass transport and associated ripening. For example, disruption into single adatoms and formation of mobile surface carbonyls [such as, *e.g.*, $Ir(CO)_2$] have been observed for clusters of Pt,[7,8] Ir,[9−11] and Rh[12] grown on TiO_2. Decay of epitaxial Cu islands on Cu(111) and Co islands on Au(111) was found to be promoted in the presence of S through formation of mobile Cu_3S_3 and Co_3S_4 complexes.[13,16,17] The lower sublimation energy of Pd−H compared to Pd was proposed to explain the Ostwald ripening of Pd clusters deposited on SiO_2 in a hydrogen atmosphere.[14] Lastly, mobile Pt_xO_y species were identified as the source of Oswald ripening of Pt particles on Al_2O_3.[15]

Here we present findings of an *in situ* scanning tunneling microscopy (STM) and X-ray photoelectron spectroscopy (XPS) sintering study, complemented by *ab initio* density functional theory (DFT) calculations. To make a molecular and atomic scale understanding of sintering possible, we have chosen an unusually well-defined cluster-support system: vapor-deposited Pt clusters on a graphene/Ir(111) moiré.[18,19] The clusters in this system are monodisperse, and each resides in an identical environment. The graphene (henceforth Gr) covers Ir(111) entirely and thereby serves as a chemically inert substrate.

* Address correspondence to gerber@ph2.uni-koeln.de.

Received for review September 11, 2012 and accepted February 4, 2013.

Published online February 04, 2013
10.1021/nn400082w

Our experiments reveal a mechanism of cluster sintering in gas atmosphere, which, to the best of our knowledge, has not yet been reported. Upon CO exposure, Pt clusters detach from the substrate and become mobile without being disrupted. Sintering takes place not by Ostwald ripening *via* volatile species formed under reaction conditions but by Smoluchowski ripening, that is, by diffusion and coalescence of the intact clusters themselves.

The "skyhook" effect on surface diffusion is a concept with a long history;[16,17,20−22] promotion of diffusion by atop adsorption of hydrogen on a metal adatom is the classic example.[21,22] However, the skyhook effect is also known in the diffusion of clusters. For example, Cu transport on Cu(111) speeds up dramatically in the presence of small surface concentrations of S. The reason is that Cu_3S_3 adclusters have a low formation energy and are mobile because their strong internal binding weakens their attachment to the substrate.[16,17] It seems plausible that adsorbed CO molecules act similarly as a skyhook for a Pt cluster on a graphene-covered Ir(111) surface. Our working hypothesis is that CO adsorption raises the cluster to a height where the potential of the underlying graphene is relatively weakly corrugated. Thus, diffusion should be facile and the observed Smoluchowski ripening a consequence.

RESULTS AND DISCUSSION

The formation of cluster arrays, like those visible in Figure 1 with a pitch of 2.53 nm, results from the template effect of the moiré formed through the mismatch of the Gr and Ir(111) surface lattices. The incommensurate C(10.32 × 10.32)/Ir(9.32 × 9.32) unit cell contains 213 C atoms bound by van der Waals forces to A_m = 87 Ir atoms. Cluster pinning occurs within the moiré cell (hcp areas, compare refs 18 and 23) where metal $d_{3z^2-r^2}$ and carbon $2p_z$ orbitals overlap. In these binding regions, 3 of the 6 C atoms in a carbon ring bind to Ir substrate atoms lying directly below and the other 3 C atoms bind to Pt cluster atoms directly above. Rehybridization of graphene to diamond-like sp^3 carbon, and thus cluster binding, relies on the presence of metal on both sides of Gr. Consequently, small Pt clusters, stable at room temperature, cannot be realized on multilayer graphene or graphite. There, Pt clusters are highly mobile unless pinned to the substrate at defects by unsaturated carbon bonds.[24,25] The clusters on the graphene moiré grow in a regular lateral arrangement (one per cell) in epitaxy with respect to the Ir(111) substrate, with their (111) planes and [110] directions parallel those of the Ir substrate. For deposited Pt amounts θ > 0.5 ML [1 ML (monolayer) corresponds to the surface atomic density of Ir(111)], the sizes of the clusters are close to a Poisson distribution,[18] while for smaller θ, the cluster size distribution is broader, mainly because of the intercell mobility of monomers and dimers during cluster growth.

Figure 1a,c,e displays STM topographs after deposition of 0.05, 0.20, and 0.44 ML Pt with average cluster sizes s_{av} = 5, 19, and 39 atoms, respectively. The average cluster size s_{av} is obtained from the known deposited amount θ (see Methods section), the fraction n of moiré cells occupied by a cluster (the filling factor), and A_m *via* $s_{av} = \theta A_m/n$.[18] With CO exposure the cluster arrays are transformed to the ones shown in the topographs to the right (Figure 1b,d,f). Full time lapse sequences of the three situations are available in the Supporting Information (movies 1−3). For clarity, locations of cluster disappearance are marked in each of the related topographs by thin white circles. Table 1 summarizes the changes by listing before and after CO exposure: the average cluster height $\bar{h}$, the fraction of moiré cells occupied n (the filling factor), as well as partial filling factors of the moiré n_1, n_2, and n_3 with one-, two-, and three-layered clusters, respectively. The data represented in Table 1 after CO exposure were obtained from STM topographs at late times when cluster sintering had terminated and a stationary state was reached.

Analysis of Figure 1 together with Table 1 yields the following conclusions: (i) CO exposure causes substantial sintering of small clusters (compare Figure 1a,b), while the effect is negligible for large clusters (compare Figure 1e,f). With increasing initial cluster size s_{av}, the reduction of n diminishes until cluster sintering vanishes for s_{av} > 50 atoms (data not shown). (ii) Cluster disappearance is primarily due to one-layered clusters, that is, the smallest clusters in the size distribution. Note that the few clusters that disappear for s_{av} = 44 (white circles in Figure 1e,f) are all one-layered ones. (iii) While for s_{av} = 5 atoms the decrease of n_1 is primarily due to cluster disappearance, for s_{av} = 39, the decrease is almost exclusively by transformation of one-layer to multilayer clusters without affecting n. (iv) As a consequence of the substantial decrease of n_1, the average cluster height increases upon CO exposure. Note that for s_{av} = 19 and 39, the cluster height distribution narrows upon CO exposure; that is, the clusters become more uniform in height.

Time lapse sequences of STM images taken during CO exposure provide insight into the mechanisms of cluster disappearance and transformation. Figure 2a,b shows two consecutive topographs during 1×10^{-9} mbar CO exposure of a 0.05 ML Pt cluster array (full sequence is provided as movie 4 in the Supporting Information). Event (i) is a movement of a cluster to a neighboring *empty* moiré unit cell. Event (ii) is a movement of a cluster to an adjacent *occupied* moiré unit cell. The one-layered clusters coalesce and form a two-layered cluster. While with adsorbed CO such cluster motion to empty and occupied neighboring moiré unit cells takes place at 300 K, substantially higher temperatures are required for cluster motion without CO.[19] The obvious conclusion from these observations is that CO exposure causes Smoluchowski ripening

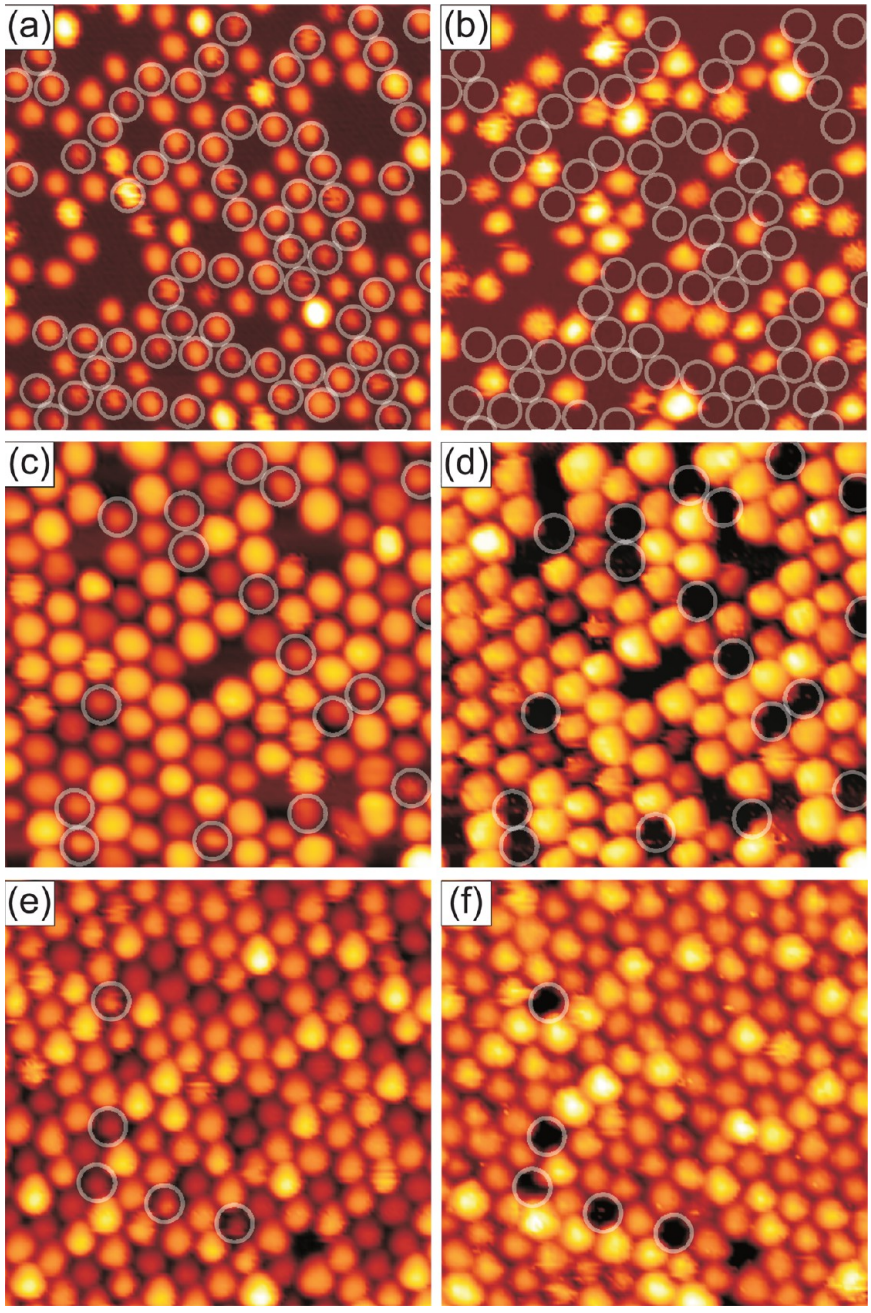

Figure 1. STM topographs of Pt cluster arrays on Gr/Ir(111) taken at the same sample location before and after exposure to CO. (a) Deposited amount $\theta = 0.05$ ML Pt; (b) as in (a) but after additional exposure to 1.1 L CO at $p_{CO} = 1 \times 10^{-9}$ mbar; (c) $\theta = 0.20$ ML Pt; (d) as in (c) but after CO exposure to 16 L, $p_{CO} = 1 \times 10^{-8}$ mbar; (e) $\theta = 0.44$ ML Pt; (f) as in (e) but after CO exposure to 20 L, $p_{CO} = 1 \times 10^{-8}$ mbar. Clusters which disappear during CO exposure and their former location are marked with circles in (a,c,e) and (b,d,f), respectively. Image size is always 290 Å $\times$ 290 Å.

(diffusion and coalescence) of clusters and thereby the reduction of *n*.

Figure 2c,d shows two consecutive STM topographs during 1×10^{-8} mbar CO exposure of a 0.20 ML Pt cluster array (full sequence is provided as movie 2 in the Supporting Information). The two encircled clusters transform from one-layered to two-layered clusters without any other changes in their environment. We name such a change toward a more three-dimensional shape *without* supply of material from other moiré cells a shape transformation.

CO-induced cluster mobility and CO-induced shape transformations are two distinct, essentially unrelated effects. It is obvious from event (i) in Figure 2b that small clusters are set in motion without a shape transformation. Also, the 0.05 ML data in Table 1 make plain that coalescence of two small one-layered clusters mostly results in a one-layered coalesced cluster. For clusters with more than 10 atoms, CO-induced cluster mobility dies off and shape transformations become the more frequent, the larger the clusters are. This can be

TABLE 1. Deposited Pt Amounts θ, Average Cluster Size s_{av}, Average Cluster Height $\bar{h}$, Filling Factors n_1, n_2, and n_3 of the Moiré Lattice with Pt Clusters of One, Two, and Three Layers High, Respectively, as Well as Their Sum n Before and After CO Exposure[a]

θ (ML)	s_{av} (atoms)	$\bar{h}$ (ML)	n_1	n_2	n_3	n
0.05 ML	5	1.09	0.75	0.07	0.00	0.82
0.05 ML + CO	10	1.24	0.34	0.11	0.00	0.45
0.20 ML	19	1.54	0.43	0.51	0.00	0.94
0.20 ML + CO	21	1.85	0.08	0.74	0.00	0.82
0.44 ML	39	1.99	0.25	0.50	0.24	0.99
0.44 ML + CO	39	2.38	0.00	0.61	0.37	0.98

[a] Analysis based on sample areas containing more than 600 moiré cells of the experiments visualized by Figure 1. Data after CO exposure were obtained when sintering had terminated.

inferred from Figure 2c,d, Table 1, and the movies of the 0.20 and 0.44 ML cluster arrays (Supporting Information).

Figure 2e displays the analysis of the filling factor n *versus* time t based on STM movies of 0.05 ML Pt cluster arrays (movies 4 and 1 in the Supporting Information). In the top panel, initially n (open squares) is constant with time within the limits of error (error primarily from STM drift). Start of exposure to 1×10^{-9} mbar CO, indicated by the gray shading, causes only a slight gradual decrease of n. It is caused by rare coalescence events. About 1500 s after the start of CO exposure (after 1.1 L CO dosed), a sharp decrease of n signifies onset of high cluster mobility and a large number of coalescence events. Then, 2000 s later the cluster density stabilizes at about half of its initial value.

In the bottom panel, a similar experiment is analyzed, where dosing of CO was performed in two parts. After a first dose of 0.4 L, only a slight decrease of n is observed. Continued imaging after pumping out CO reveals no further change in the cluster array. Reopening the CO valve and dosing of CO also displays no significant changes in n until the second dose reaches 0.7 L (the integral dose reaches 1.1 L). Closing the CO valve immediately after the onset of cluster mobility and coalescence does not impede the ripening process. Instead, n continues to decrease with the same time behavior and to a similar level, as observed in the top panel in the presence of CO.

It must be concluded that after a threshold exposure of about 1.1 L the properties of the Pt clusters are changed to an extent that they are mobile, irrespective of the continued presence of gas. As CO is known to adsorb on Pt at 300 K and to desorb only with negligible rates, we conclude that the threshold dose is related to a threshold coverage. Moreover, our experiment makes clear that the heat of CO adsorption on the Pt clusters is irrelevant for cluster mobility.

Donner and Jakob[26] investigated tip-induced cluster manipulation in some detail and pointed out that high tunneling resistances, $R \approx 2 \times 10^9$ Ω, are necessary to avoid Pt cluster pick-up and lateral displacement on graphene on Ru(0001). Early on, we used an STM tip

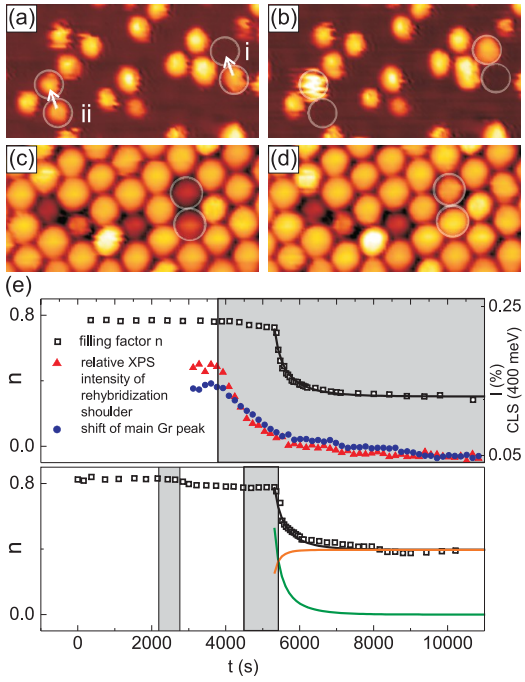

Figure 2. (a,b) Consecutive STM topographs after deposition of 0.05 ML Pt during CO exposure at 1×10^{-9} mbar. Time between images $\Delta t = 53$ s. Stills from movie 4 in the Supporting Information. (c,d) Consecutive STM topographs after deposition of 0.20 ML Pt during 1×10^{-8} mbar CO exposure. Time between images $\Delta t = 53$ s. Stills from movie 2 in the Supporting Information. (e) Filling factor n (black open squares) as a function of time t for cluster arrays formed by deposition of 0.05 ML Pt. Times of exposure by 1×10^{-9} mbar CO are indicated by gray shading. Full black lines are model fits (see text). Data for top and bottom panel were taken from movie 4 and movie 1, respectively. In the top panel, additionally the relative XPS intensity I of the C 1s component related to cluster binding (right axis, red upward triangles) and the core level shift of the main C 1s peak (right axis, blue full dots) are plotted *versus* t for a 0.05 ML Pt cluster array. Data shifted on t-axis such that the start of 1×10^{-9} mbar CO exposure matches with the one from STM movie in the same panel. In the bottom panel, additionally fractions n_m of mobile (green line) and n_i of immobile (orange line) clusters according to model fit are plotted (see text).

similarly, as a tool for Ir cluster removal from graphene on Ir(111).[18] Thus, it is natural to ask how significantly the results we present in Figure 1 and Figure 2 were affected by tip−cluster interaction. Indeed, we found as well that the probability for tip−cluster interaction decreases monotonically with R and therefore used $R \geq 2 \times 10^{10}$ Ω throughout. Under these conditions, cluster manipulation by the STM tip is a very rare event. Indeed, close inspection of movies 1−4 provided as Supporting Information reveals that occasional tip−cluster interaction events were present, specifically once the clusters are mobilized by CO. Areas scanned only twice, before CO exposure and after sintering had terminated, show only slight differences for n and the n_i compared to areas that were continuously scanned more than 150 times during CO exposure (compare Figure 1 of the Supporting Information for a quantitative analysis). Thereby, it can be ruled out that the Smoluchowski

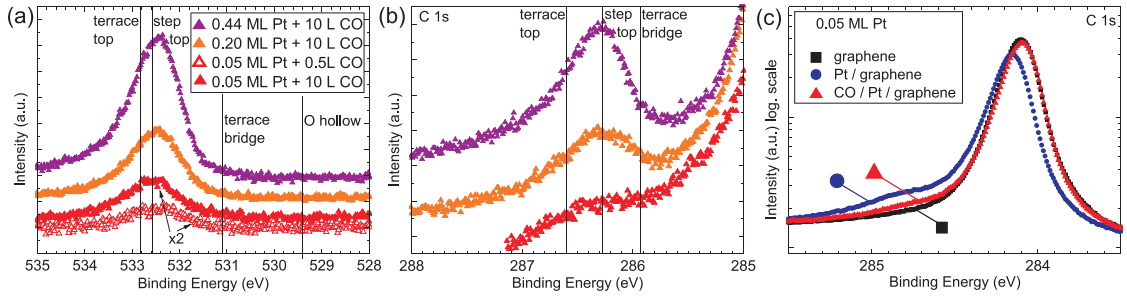

Figure 3. (a) O 1s spectra of 0.5 L CO adsorbed on 0.05 ML (open red) and 10 L CO adsorbed on 0.05 ML (red), 0.20 ML (orange), and 0.44 ML (purple) Pt cluster arrays. Core level binding energies for CO adsorbed in terrace atop, terrace bridge, and step atop sites on Pt(355)[28] as well as for oxygen adsorbed on Pt(111)[29] are indicated. Spectra are shifted vertically for clarity. (b) C 1s fingerprint region region of C atoms in CO after exposure of 0.05, 0.20, and 0.44 ML Pt cluster arrays to 10 L CO. Binding energies for CO adsorbed in terrace atop, terrace bridge, and step atop sites on Pt(332)[30] are indicated. Spectra are shifted vertically for clarity. (c) C 1s spectra of pristine Gr/Ir(111) (black), Gr/Ir(111) with 0.05 ML Pt cluster array (blue), and Gr/Ir(111) with 0.05 ML cluster array after exposure to 10 L CO at 300 K (red). All 10 L CO exposures were done at $p_{CO} = 1 \times 10^{-7}$ mbar, and 0.5 L CO was dosed at $p_{CO} = 1 \times 10^{-9}$ mbar.

ripening observed dynamically in the STM movies was caused by tip−cluster interactions. The quantitative analysis provided in Table 1 was conducted on areas that were at most scanned twice, before CO exposure and after sintering had terminated. Thereby, tip effects are eliminated. All general features derived from Table 1 are present in all experiments conducted. However, specifically for 0.05 ML cluster arrays, some variation in the initial filling factors n and n_i was observed from experiment to experiment, depending on the graphene quality and the deposition conditions (see below).

To summarize, our experiments provide unambiguous evidence that cluster sintering proceeded by Smoluchowski ripening only. In the entire data taken, not a single event of a gradual disappearance of a cluster was observed. Clusters always moved and disappeared as integral entities as shown in Figure 2. The observation that clustering sintering ceases, irrespective of whether CO is supplied continuously or not, is consistent with this view. If Smoluchowski ripening prevails, cluster sintering stops once the clusters have become too large to detach from the substrate to move (see below for a more detailed discussion), as observed. If Ostwald ripening would prevail, it would be hard to understand why the formation of mobile carbonyl species abruptly stops if clusters have reached a certain size.

In previous work, we described[19] cluster hopping with a rate ν as a thermally activated process: $\nu = \nu_0 e^{E_a/k_B T}$. Here k_B, T, E_a, and ν_0 are the Boltzmann constant, temperature, activation energy, and attempt frequency for a move, respectively. With the simplifying assumption of identical diffusion properties for the entire cluster ensemble, we were able to obtain quantitative estimates for E_a and ν_0 using the temperature dependence of ν as obtained from isochronal annealing sequences. Here we extend this approach to describe adsorption-induced cluster mobility. After the threshold exposure of CO, we assume a cluster to be within one of the two classes: it belongs either to the fraction n_m of mobile clusters or to the fraction n_i of clusters that could not be mobilized by CO. The decrease of n_m with time is then

$$\frac{dn_m}{dt} = -\nu n_m n_i - \nu 2 n_m n_m$$

The first term describes the decrease of n_m by coalescence of a mobile cluster with an immobile cluster; the second term is the decrease by coalescence of two mobile clusters. In the latter term, the factor 2 takes into account that the formation of *one* immobile cluster consumes *two* mobile clusters.[27] Similarly, the increase of n_i is then

$$\frac{dn_i}{dt} = \nu n_m n_m$$

This system of nonlinear differential equations is solved numerically. The sum of the starting values $n_i(0) + n_m(0)$ equals the initial filling factor $n(0)$ obtained from the experimental data. The ratio $n_m(0)/n_i(0)$ as well as ν are fitting parameters.

The black lines in Figure 2e are excellent fits to the experimental $n(t)$. The fit parameters are $\nu = 4 \times 10^{-3}$ Hz and $n_m(0)/n_i(0) = 6.2$ for the top panel as well as $\nu = 4 \times 10^{-3}$ Hz and $n_m(0)/n_i(0) = 2.12$ for the bottom panel. The fact that the same hopping rate fits both experiments lends credence to our description. In the bottom panel, the solution $n(t)$ is also separated into its constituents $n_m(t)$ (green) and $n_i(t)$ (orange). The ratio $n_m(0)/n_i(0)$ differs between the top and the bottom panel fit. Inhomogeneities in the initial cluster size distribution or the fact that CO was pumped out after reaching the threshold dose in the bottom panel experiment might cause this difference.

To relate the CO exposure-induced Pt cluster dynamics to adsorption properties and cluster binding, we conducted high-resolution XPS experiments and measured O 1s spectra of the O atoms in CO and C 1s spectra of the C atoms in CO and in Gr. No O 1s peak intensity was detected on pristine Gr/Ir(111) after CO exposure, consistent with the absence of CO adsorption on Gr/Ir(111). The lowest spectrum in Figure 3a

(open red triangles) displays the O 1s region of the photoelectron spectrum measured after exposure of a 0.05 ML cluster array to 0.5 L CO. It corresponds to the situation before cluster coalescence, which sets in only after exposure to the threshold dose of 1.1 L. The three other spectra were measured after 10 L CO exposure of 0.05, 0.20, and 0.44 ML Pt cluster arrays. They correspond to situations where cluster coalescence had already taken place (right column of Figure 1). With increased Pt deposition, the O 1s peak area and thus the amount of adsorbed CO increases, as might be expected. The O 1s peak position is independent of whether cluster coalescence had taken place or not (0.05 ML array, bottom two spectra) and of the deposited amount (top three spectra). This suggests an identical CO adsorption site for all situations. We indicate the O 1s binding energies for CO adsorbed in terrace atop, terrace bridge, and step atop sites on Pt(355)[28] by vertical lines in Figure 3a.[31] Since the O 1s photoelectron binding energies are rather sensitive to the adsorption geometry of CO, the comparison with our measured value suggests that the CO molecules are adsorbed atop at the cluster edge atoms. Adsorption of oxygen (and thus dissociation of the CO molecule) can be ruled out by absence of a feature at 529.4 eV[29] (vertical line "O hollow" in Figure 3a), which would be present for O adsorbed in the 3-fold hollow sites on Pt. Note that when clusters start to develop larger terraces, owing to their size and by coalescence, a shoulder at the terrace bridge bonded position starts to develop in the O 1s spectrum. We observed this for a 0.75 ML cluster array (data not shown). Since bridge bonding is present on Pt(111) terraces after saturation with CO, this could have been anticipated. Figure 3b displays the C 1s fingerprint region of C atoms in CO after exposing 0.05, 0.20, and 0.44 ML Pt cluster arrays to 10 L CO. The strongly asymmetric shape of the background is due to the C 1s peak of graphene located at 284.1 eV to be discussed later (compare Figure 3c). Consistent with the O 1s spectra, also for the C 1s spectra, the peak position is independent of the deposited amount and confirms identical adsorption sites for all three cases. The comparison between our C 1s spectra and those measured for CO adsorbed in terrace atop, step atop, and bridge sites on Pt(332)[30] indicates that CO adsorbs on step atop Pt sites, consistent with our inferences based on the O 1s spectra. However, adsorption on terrace atop sites cannot be excluded entirely.

In conclusion, our photoelectron spectra provide evidence that for cluster arrays with sizes $s_{av} < 40$ atoms CO adsorbs atop. This finding is consistent with the adsorption behavior of CO on small, free Pt clusters in a beam with sizes up to 22 atoms. Gruene *et al.* demonstrated that for such Pt clusters the CO adsorption is exclusively atop.[33] Also the work of Tränkenschuh *et al.*[28,32] provides unambiguous evidence that the atop site is the preferred adsorption site of CO molecules at steps and on terraces.

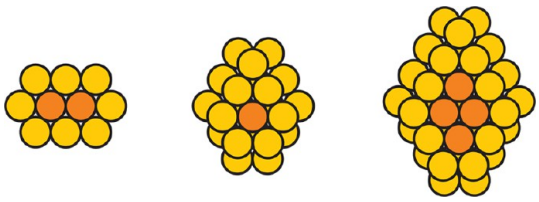

Figure 4. Ball models for Pt clusters containing 10, 22, and 38 atoms. Edge atoms are colored yellow, terrace atoms orange.

An estimate for the average number of adsorbed CO molecules per cluster after saturation was obtained from O 1s intensities calibrated to the O 1s signal originating from a CO ($\sqrt{3} \times \sqrt{3}$)R30° layer on bare Ir(111) with a coverage of 0.33 ML.[34] We obtain 8, 15, and 27 CO molecules per Pt cluster for the 0.05, 0.20, and 0.44 ML arrays, respectively. According to Table 1, we find 8 CO molecules adsorbed to a cluster with s_{av} = 10 atoms, 15 CO molecules to one with s_{av} = 21 atoms, and 27 CO molecules to one with s_{av} = 39 atoms. Ball models for representative clusters of average or close to average size after CO exposure are shown in Figure 4. For all three cases, the number of edge atoms (yellow) coincides very well with the estimated number of adsorbed CO molecules. We conclude that at saturation to good approximation each cluster edge atom accommodates one CO molecule.

Figure 3c displays the C 1s region of Gr/Ir(111) before (black) and after (blue line) room temperature deposition of 0.05 ML Pt. For Gr/Ir(111), the spectrum is fitted with a single C 1s peak located at 284.1 eV with a full width at half-maximum (FWHM) of 0.22 eV.[35] The Pt deposition is associated with the development of a broad shoulder in the binding energy range of 284.3−285 eV. Previously, we found this shoulder component to be due to C atoms under and in the vicinity of the Pt clusters. As a consequence of cluster binding, these C atoms are sp^3-hybridized and close to Ir(111) at chemical rather than van der Waals binding distance. For these atoms, we demonstrated a linear relationship between their core level shift and their height above Ir(111). In addition, we observe a +50 meV shift of the main peak which we assign to doping by the Pt clusters.[35] The C 1s spectrum after exposing the 0.05 ML cluster array to 10 L CO is displayed in Figure 3c as red upward triangles. The rehybridization shoulder largely disappeared, and the main peak shifts back to the position of Gr/Ir(111) without Pt clusters. Similar data are provided in the Supporting Information for 0.20 and 0.44 ML Pt cluster arrays.

The diminished rehybridization shoulder and the backshift of the Gr main peak are not a consequence of cluster mobility; that is, they do not originate from the decrease of n and the ensuing reduced contact area of the clusters with Gr. The time-dependent

analysis of the integral intensity of the C 1s rehybridization shoulder (red triangles in Figure 2e, top panel; see Supporting Information for details of fitting) and the binding energy shift of the C 1s Gr main peak (blue dots in Figure 2e) show that both quantities decrease immediately after the start of the CO exposure, while *n* is still nearly constant. When cluster mobility sets in, both quantities are already reduced by more than 50%.

Thus, our experiments show that the adsorption of CO molecules on Pt cluster edge atoms largely undoes graphene rehybridization beneath the cluster before sintering starts. What can be the origin of this effect?

Consistent with studies on vicinals to Pt(111) and Pt clusters, where CO prefers to reside in 1-fold edge sites,[28,32,33] our XPS experiments say that CO binds atop Pt cluster edge atoms. In such sites, one can expect that a graphene C atom, the cluster Pt atom, and the CO molecule will be almost collinear. According to Blyholder, CO−Pt bond formation then occurs as a result of charge donation from the σ molecular orbital of CO to Pt sp-bands and back-donation of Pt d-electrons into the $2\pi^*$ CO orbital.[36,37]

Such bonding *cannot lead to a skyhook effect*. The problem, as Föhlisch *et al.*'s elaboration of the Blyholder model makes clear, is that CO adsorption in a 1-fold site does not imply a competition for Pt($5d_{3z^2-r^2}$) electrons.[38,39] The Pt($5d_{3z^2-r^2}$) orbital is involved in binding the Pt to the underlying graphene. So, a weakening of the interaction of the Pt($5d_{3z^2-r^2}$)−C($2p_z$) might well lead to a mobilization of a Pt island, but on the basis of our current understanding of CO binding to Pt atop sites, such weakening does not occur.

The reason is that "back-donation" into the CO $2\pi^*$ orbital is the result of hybridization with Pt($5d_{xz}$) and Pt($5d_{yz}$) electrons, that is, $5d_\pi$ electrons, not Pt($5d_{3z^2-r^2}$) electrons. They have the wrong (5σ) azimuthal symmetry for forming hybrids with the CO $2\pi^*$. In fact, Föhlisch *et al.* showed that the interaction between the CO σ and the Pt($5d_{3z^2-r^2}$) orbital is repulsive. Thus, it is not conducive to a competition that would weaken the Pt bond to the graphene below.

First-principles calculations based on the local density approximation confirm this picture but, as we will explain, do not yet permit a definitive interpretation of the Smoluchowski coarsening we have observed, given available experimental information and the theoretical state-of-the-art.

Previously, we have used DFT calculations successfully to gain insight into cluster binding on graphene on Ir(111) and were even able to reproduce core level shifts of graphene atoms due to Pt cluster binding with good accuracy.[23,35] Therefore, despite experience suggesting that DFT will not show a preference for CO bonding in the observed 1-fold edge sites on the Pt/Gr/Ir(111) clusters,[40] we undertook *ab initio* calculations to see whether they might nevertheless help to explain how CO mobilized our Pt islands. The particulars of our

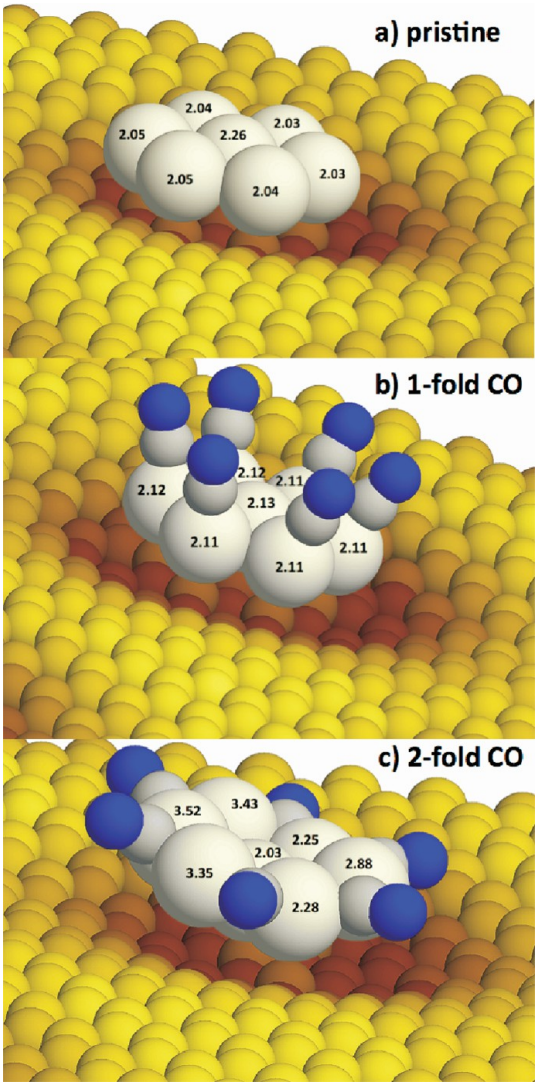

Figure 5. Geometries of a planar Pt heptamer adsorbed to the hcp area of graphene on Ir(111). (a) Pristine Pt heptamer; (b) Pt heptamer decorated by CO molecules in 1-fold (atop) sites; (c) Pt heptamer decorated by CO molecules in 2-fold (bridge) sites. Gray and blue spheres represent C and O atoms of the CO molecules. White spheres are Pt atoms, and small, yellow to brown ones are the C atoms of the Gr layer. Browner means closer to the underlying Ir(111) substrate, and yellower means higher above it. The numbers are computed distances, in Å, of each Pt atom from the nearest C atom below it.

VASP[41,42]/PAW[43,44]/LDA[45,46] calculations were just as reported by Knudsen *et al.*,[35] except that six CO molecules were added to an island comprising 7 Pt atoms in the Gr/Ir(111)-(9 × 9) moiré unit cell.

Figure 5a displays the geometry resulting from a DFT optimization of a pristine Pt heptamer. Note that the graphene beneath the cluster is buckled. Directly below each Pt atom is a relatively yellow (*i.e.*, high-lying) C atom, to which it is bound at a distance of about 2.16 Å, the sum of the covalent radius of C and the metallic radius of Pt. Between the raised C atoms are relatively brown (*i.e.*, lower-lying) ones. They are bound to Ir atoms below them and lie at chemical

bonding distances from them. The buckling implies that underneath the cluster the graphene has locally rehybridized from sp^2 to diamond-like sp^3 carbon.[23]

In Figure 5b, we show the results of optimizing a Pt cluster with CO molecules 1-fold bound to cluster edge atoms, the coordination required for correspondence with our XPS data. The molecules did not shift away from the 1-fold sites in the course of structural relaxation, indicating a relative minimum in the energy, but CO adsorption only caused distances between Pt atoms and C atoms to increase marginally, by less than 0.07 Å on average, and left the Pt−C chemical bonds intact for all seven Pt atoms. Correspondingly, the underlying Gr remained buckled, locally, with C atoms alternately yellowish because they have moved up to bind to Pt atoms and brown because they have moved down to bind to underlying Ir atoms. Thus, if the pristine cluster is immobile, then the cluster decorated by CO molecules in 1-fold edge sites is equally so, according to DFT. This result is entirely consistent with the conclusions we have drawn from the study of CO binding in 1-fold sites on Pt(111) by Föhlisch *et al.*,[38,39] although, regrettably, the weight of the experimental evidence implies that atop CO is what undoes the binding of Pt to C, mobilizing the Pt clusters.

Despite the experimental evidence for 1-fold CO adsorption on the edges of our Pt clusters, we also investigated CO in edge bridge sites, which, based on DFT studies of CO on vicinals to Pt(111), we expected to provide stronger bonding.[40] As expected, the bridging geometry was energetically preferred over 1-fold cluster decoration, the preference amounting to 81 meV per CO, or 0.49 eV/island. Surprisingly, however, the bonding within the graphene and between graphene and the Pt cluster as shown in Figure 5c changed remarkably compared to Figure 5a,b. Upon bridging CO adsorption, distances between Pt atoms and C atoms increased substantially, by more than 0.90 Å on average. Four of the Pt atoms moved too far from the nearest C atoms to be chemically bound to them, and correspondingly, the underlying graphene unbuckled. Only two edge Pt atoms remained at a chemical binding distance (still about 0.25 Å higher than for the pristine case), for instance, in Figure 5c, the one at the front of the cluster labeled "2.28". The unbuckling of the underlying graphene implies diminished rehybridization of graphene, in line with our experimental observations (compare Figure 3c), and, likely, with facile cluster mobilization.

Incidentally, despite the dramatically increased bond distances between the Pt and the underlying C atoms, the effect of adsorption on the bond lengths within the Pt cluster is marginal. The average Pt−Pt distance increased upon CO adsorption by just 2%, from 2.62 to 2.67 Å. Apparently, the cluster integrity was not affected by CO adsorption.

Thus, the DFT calculation for what appears to be the experimentally wrong 2-fold adsorption site is consistent with a skyhook effect, whereas that for the observed 1-fold adsorption geometry offers no explanation for CO-induced cluster mobilization. In the DFT optimization, bridging CO adsorption caused (i) substantially weakened and lengthened bonds between Pt atoms and the underlying C atoms, (ii) a lifting of the rehybridization or an unbuckling of the graphene, and (iii) an only negligible effect on the bond strength within the cluster itself. These three observations imply cluster mobility, as observed. The Pt atoms moved away from the graphene. At the same time, the underlying substrate potential presumably became less corrugated and lateral diffusion more facile.

This discussion underlines a need for technical improvements in theory and further experiments. The, by now, well-known deficiency of approximate density functionals has once again manifested itself in our prediction that CO will prefer to bind in a higher rather than a lower coordination geometry on a metallic substrate, in this case a 7 atom Pt island. On the other hand, the calculated preference for the 2-fold bonding geometry is small, and there is no reason to assume that the nature of the CO bonds would be appreciably different in an improvement over current DFT more faithful to observed binding energies. Assuming that DFT does describe the nature of the CO−Pt bonds in a qualitatively correct way, and assuming that the edge-saturated 7 Pt atom islands are representative, then it seems necessary to conclude that island mobilization occurs when CO transiently resides in edge bridge sites. On the other hand, we have no experimental evidence for transient, bridge-bonded CO. Further experiments, perhaps in the nature of IR spectroscopy, would be helpful in this regard. They might reveal a population of CO in bridge sites or rule that possibility out.

Before leaving the DFT results, we wish to remark on the locality of the unbinding effect and its likely relation to the cluster size dependence of CO-induced mobility. The key observation is that only Pt atoms on which CO is adsorbed lose their coordination to the underlying graphene.

Given this locality of the unbinding effect, let us revisit Table 1. It says that after CO exposure sintering terminates and clusters are immobile once they reached a size of $s = 10$ atoms. As shown in Figure 4, a compact 10 atom cluster has 8 edge atoms. In agreement with our XPS coverage analysis, these 8 edge atoms possess 8 adsorbed CO molecules, either atop bonded (as found in experiment) or bridge bonded (as predicted by DFT). Now we postulate that the effect of the adsorbed CO molecules is localized to their Pt atom counterparts, which unbind from the graphene. This means a 10 Pt atom cluster, whose edges are saturated by CO, is immobilized by its two terrace atoms. From that, we deduce that a cluster of as few as two Pt atoms will not diffuse, and that one should expect the initial CO-free system, with an

average cluster size of s_{av} = 5 atoms for the 0.05 ML cluster array, to be stable. By contrast, after enough CO has been deposited that there are decorated clusters with just one undecorated Pt atom, or none, then these decorated clusters will be mobilized. Smoluchowski ripening will proceed, accordingly, until their coalescence creates larger clusters with at least two CO-free Pt atoms. At that point, ripening will cease.

A 38 atom 2-layered Pt cluster, characteristic for the 0.44 ML Pt cluster arrays with s_{av} = 39, possesses 9 atoms in the first layer, which are buried by second layer Pt atoms (compare Figure 4). These atoms are protected against CO adsorption, and thus the stability of the 0.44 ML cluster array is understandable. In the 0.20 ML cluster array, still some CO-induced mobility is observable for s_{av} = 19 atoms initially. We attribute this to the tail of the cluster size distribution extending below 10 atoms. The observation that most of the clusters that become mobile upon CO adsorption in the 0.20 ML case are 1-layered clusters is at least consistent with the assumption that these are the smallest ones in the distribution.

Whereas lateral motion is the most relevant CO-induced process for small clusters, for those with more than 20 Pt atoms, shape transformations to more three-dimensional arrangements dominate and proceed without mass exchange between clusters. Generally, the shape of a supported cluster is determined by the balance of substrate surface, cluster surface, and interface energy.[47] The substrate surface energy can be neglected here, as the surface free energy of graphene is very low owing to its inertness. Even without CO adsorbed, upon cluster growth, initially 1-layered clusters transform to 2-layered clusters.[19,48] As the rehybridization area of graphene is limited in size, at some point in the growth process, the increase of the interface area is disfavored compared to an increase of cluster cohesion (lowering of total surface energy). Therefore, arriving Pt atoms do not stay at the cluster edge in contact with graphene but prefer to increase their coordination with other Pt atoms by forming a second layer.[48] Consider now a cluster somewhat below the critical size s_c, which is around 19 atoms for a Pt cluster on Gr/Ir(111) (compare Table 1). CO adsorption will change its shape because the binding of the edge atoms to their underlying C atom counterparts is substantially weakened. Therefore, interface formation is disfavored compared to an increase of Pt cohesion. Thus, a 2-layered configuration will already be preferred for a smaller size $s_c' < s_c$. Note that CO adsorption will also affect Pt−Pt bonding. However, since in Pt−Pt bonding all valence electrons are already involved, the effect of an adsorbed CO will be much smaller than for the Pt−C bonding.

The preferential adsorption of CO to low coordinated atoms has an additional effect on cluster energetics and also tends to favor more three-dimensional shapes. Consider a 19 atom planar cluster with CO-saturated edges and a surplus of a few less strongly bound terrace CO molecules. Transformation of the 1-layered cluster into a 2-layered cluster increases the number of strongly binding edge atoms. Through this shape transformation, the terrace surplus CO molecules can bind more strongly to the newly formed edge atoms, which in turn reduces the cluster surface energy. The cluster thus reshapes to provide as many favorable adsorption sites as possible.

Reshaping of stepped Pt surfaces into nanometer-sized Pt clusters was found under an applied CO pressure in the millibar range.[49] This reshaping was interpreted to be driven by a reduction of the repulsion of adjacent CO molecules. While we cannot entirely rule out a contribution of this effect, the CO-induced Pt−C bond weakening and the enhanced CO binding by cluster reshaping appear to be a straightforward explanation for the similar phenomenon we observe here.

We also exposed 0.05 ML Pt cluster arrays on Gr/Ir(111) to H_2 and O_2. Even large exposures of the order of 1000 L did not induce cluster mobility. A problem for the near future is to rationalize the different behavior of the Pt clusters with respect to these gases, likely in terms of different O and H atom bonding geometries.[50,51]

Lastly, we consider why the majority of Pt clusters in the 0.05 ML arrays are set in motion after a well-defined threshold exposure (compare Figure 2e). Above we argued that clusters begin to move when fewer than 2 atoms are left without a CO molecule atop. This requires a larger cluster (*e.g.*, a flat 8 atom cluster) to collect more CO molecules than a smaller one needs (*e.g.*, a 5 atom cluster). The larger CO capture efficiency of a larger cluster, most likely in proportion to its area, helps to synchronize the moment when larger and smaller clusters become mobile. However, it is questionable whether this compensation effect is fully able to explain the observed synchronization for the onset of cluster motion. One possibility is that the local graphene strain field associated with a moving cluster might slightly affect clusters in its vicinity and thereby help to synchronize cluster mobility.

An implication of the CO-induced cluster mobility is the sensitivity of Pt cluster array growth to the CO background pressure. Small clusters of a few Pt atoms are abundant during growth and become more mobile by CO adsorption. As a consequence, in a poor vacuum with residual CO, arrays that are less regular form, with a smaller filling factor.

Figure 6a displays an STM topograph after deposition of 0.10 ML Pt under ultrahigh vacuum conditions with the total background pressure during deposition below 2×10^{-10} mbar. Here graphene was prepared by room temperature ethylene adsorption until saturation, followed by thermal decomposition at 1450 K, but without additional exposure to ethylene at elevated temperatures. This results in graphene flakes covering a fractional

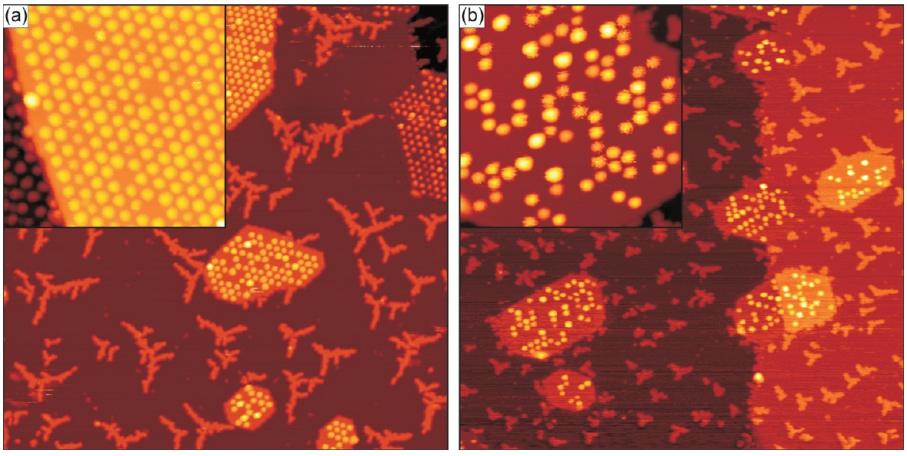

Figure 6. STM topographs after deposition of 0.10 ML Pt on Gr/Ir(111). (a) Deposition in a partial CO pressure of $p_{CO} < 2 \times 10^{-10}$ mbar. (b) Deposition with $p_{CO} = 5 \times 10^{-9}$ mbar. Image sizes 1650 Å × 1650 Å, inset sizes 375 Å × 375 Å.

surface area of about 20%.[52] The inset shows the cluster array with a filling factor $n = 0.92$ and with predominantly 1-layered clusters, as expected under these conditions.[19] On the bare Ir surface, fractal dendritic Pt islands are visible.

Figure 6b displays an STM topograph of the same experiment, except that during Pt growth a CO pressure of $p_{CO} = 5 \times 10^{-9}$ mbar was applied. The inset highlights the poor filling of the moiré with $n = 0.42$ and with a larger relative fraction of 2-layered clusters. The Pt islands on the bare Ir surface are smaller and display a significantly higher island number density. This is expected for epitaxial growth of Pt in the presence of CO.[53]

CONCLUSIONS

We have shown that CO-induced sintering of small Pt clusters on Gr/Ir(111) may be traced back to Smoluchowski ripening. Even if clusters stay immobile upon adsorption, they often transform to a more three-dimensional shape. In photoelectron spectroscopy, the CO adsorption on the Pt clusters is signaled by a pronounced decrease of a shoulder in the C 1s peak, characteristic for graphene rehybridization. CO is found to be adsorbed atop on Pt cluster edge atoms. We had hoped that DFT calculations would help to interpret our discovery of island mobility, but instead, they have left us in a quandary. Either we disbelieve the DFT result that CO in 1-fold island edge sites has little effect on the bonding of the Pt to the graphene below, or we must assume that a CO-decorated island can adopt a transient structure in which Pt−graphene bonds are broken and the island is mobilized. In the first case, we lack theoretical evidence to justify the disbelief. In the latter, we lack experimental confirmation of transient configurations. Evidently, a result of the work reported here is to establish directions for future research efforts. The possible payoff in the form of novel catalytic systems makes that seem more than worthwhile.

METHODS

STM experiments were carried out in the TUMA-III Laboratory in Cologne, and XPS experiments were conducted at Beamline I311 at the MAX-IV Laboratory[54] in Lund using identical sample preparation procedures. The base pressure in both ultrahigh vacuum systems is below 1×10^{-10} mbar. The sample was cleaned by repeated cycles of sputtering at 300 K and annealing to 1400−1500 K. Graphene was prepared by room temperature ethylene (C_2H_4) adsorption until saturation, thermal decomposition at 1450 K, and subsequent 1200 s exposure to 1×10^{-7} mbar ethylene at 1170 K resulting in a well-oriented, perfectly closed, single layer of graphene.[55] Low-energy electron diffraction of the graphene layer confirms the excellent orientation order of Gr: the dense packed rows of Ir(111) and Gr are aligned. Rotational variants of Gr were absent.[56] Pt cluster growth on Gr/Ir(111) was conducted at 300 K by e-beam sublimation of degassed high-purity Pt. The deposition rate was 3×10^{-2} ML/s, where 1 ML (one monolayer) corresponds to the surface atomic density of Ir(111). During deposition, the pressure remained in the low 10^{-10} mbar range.

In the variable-temperature STM system, the Pt evaporator was calibrated by determination of the fractional area of monolayer Pt islands resulting from deposition onto clean Ir(111). STM imaging was conducted at room temperature. STM topographs were postprocessed using the WSxM software.[57] Tunneling resistances of $\approx 2 \times 10^{10}$ Ω are used to avoid tip−cluster interaction. Moreover, owing to the convolution of the tip shape with the clusters, multilayered clusters tend to display a larger base area compared to 1-layered ones.

The XPS spectra were collected in normal emission with an angular acceptance of ±5°. For C 1s and O 1s spectra, we used photon energies of 390 and 650 eV, respectively. All spectra are normalized to the background, and core binding energies, defined to have positive values, are referenced to the Fermi edge. Accordingly, a positive core level shift corresponds to a binding energy increase. At the I311 beamline, the same Pt evaporator as in the TUMA-III Lab with identical settings and distance to the sample was used. The STM rate calibration was confirmed using the Ir 4f surface peak, which vanishes at 1 ML coverage. Both calibrations agree within 10%.

Conflict of Interest: The authors declare no competing financial interest.

Acknowledgment. Funding by DFG through the project MI581/17-2, the Swedish Research Council, and the Danish Council for Independent Research, as well as support by the

MAX-IV Laboratory staff is gratefully acknowledged. Work by P.J.F. was supported by the U.S. DOE Office of Basic Energy Sciences, Division of Materials Science and Engineering. Sandia is operated by the Lockheed Martin Co. for the U.S. Department of Energy's National Nuclear Security Administration under Contract DE-AC04-94AL85000.

Supporting Information Available: STM movies showing the Pt cluster arrays exposed to CO (Figures 1 and 2), two additional figures, and a quantitative analysis related to the relevance of tip−cluster interactions, XPS data similar to Figure 3c but for higher Pt coverages, as well as details of the fitting procedure for the XPS C 1s spectra. This material is available free of charge *via* the Internet at http://pubs.acs.org.

REFERENCES AND NOTES

1. Heiz, U., Landman, U., Eds. *Nanocatalysis*; Springer-Verlag: Berlin, 2007.
2. Lopez, N.; Janssens, T. V. W.; Clausen, B. S.; Xu, Y.; Mavrikakis, M.; Bligaard, T.; Nørskov, J. K. On the Origin of the Catalytic Activity of Gold Nanoparticles for Low-Temperature CO Oxidation. *J. Catal.* **2004**, *223*, 232–235.
3. Heiz, U.; Sanchez, A.; Abbet, S.; Schneider, W.-D. Catalytic Oxidation of Carbon Monoxide on Monodispersed Platinum Clusters: Each Atom Counts. *J. Am. Chem. Soc.* **1999**, *121*, 3214–3217.
4. Campbell, C. T.; Parker, S. C.; Starr, D. E. The Effect of Size-Dependent Nanoparticle Energetics on Catalyst Sintering. *Science* **2002**, *298*, 811–814.
5. Bartholomew, C. H. Mechanisms of Catalyst Deactivation. *Appl. Catal. A* **2001**, *212*, 17–60.
6. Sehested, J.; Gelten, J. A. P.; Remediakis, I. N.; Bengaard, H.; Nørskov, J. K. Sintering of Nickel Steam-Reforming Catalysts: Effects of Temperature and Steam and Hydrogen Pressures. *J. Catal.* **2004**, *223*, 432–443.
7. Berkó, A.; Szöko, J.; Solymosi, F. Effect of CO on the Morphology of Pt Nanoparticles Supported on TiO_2(110)-(1 × *n*). *Surf. Sci.* **2004**, *566*−*568*, 337–342.
8. Raskó, J. CO-Induced Surface Structural Changes of Pt on Oxide-Supported Pt Catalysts Studied by DRIFTS. *J. Catal.* **2003**, *217*, 478–486.
9. Berkó, A.; Solymosi, F. CO-Induced Changes of Ir Nanoparticles Supported on TiO_2 (110)-(1 × 2) Surface. *Surf. Sci.* **1998**, *411*, L900–L903.
10. Berkó, A.; Solymosi, F. Effects of Different Gases on the Morphology of Ir Nanoparticles Supported on the TiO_2 (110)-(1 × 2) Surface. *J. Phys. Chem. B* **2000**, *104*, 10215–10221.
11. Solymosi, F.; Novak, E.; Molnar, A. Infrared Spectroscopic Study on Carbon Monoxide-Induced Structural Changes of Iridium on an Alumina Support. *J. Phys. Chem.* **1990**, *94*, 7250–7255.
12. Berkó, A.; Solymosi, F. Adsorption-Induced Structural Changes of Rh Supported by TiO_2 (110)-(1 × 2): An STM Study. *J. Catal.* **1999**, *183*, 91–101.
13. Kibsgaard, J.; Morgenstern, K.; Lægsgaard, E.; Lauritsen, J. V.; Besenbacher, F. Restructuring of Cobalt Nanoparticles Induced by Formation and Diffusion of Monodisperse Metal−Sulfur Complexes. *Phys. Rev. Lett.* **2008**, *100*, 116104.
14. Di Vece, M.; Grandjean, D.; Van Bael, M. J.; Romero, C. P.; Wang, X.; Decoster, S.; Vantomme, A.; Lievens, P. Hydrogen-Induced Ostwald Ripening at Room Temperature in a Pd Nanocluster Film. *Phys. Rev. Lett.* **2008**, *100*, 236105.
15. Simonsen, S. B.; Chorkendorff, I.; Dahl, S.; Skoglundh, M.; Sehested, J.; Helveg, S. Direct Observations of Oxygen-Induced Platinum Nanoparticle Ripening Studied by *In Situ* TEM. *J. Am. Chem. Soc.* **2010**, *132*, 7968–7975.
16. Feibelman, P. J. Formation and Diffusion of S-Decorated Cu Clusters on Cu(111). *Phys. Rev. Lett.* **2000**, *85*, 606–609.
17. Ling, W. L.; Bartelt, N. C.; Pohl, K.; de la Figuera, J.; Hwang, R. Q.; McCarty, K. F. Enhanced Self-Diffusion on Cu(111) by Trace Amounts of S: Chemical-Reaction-Limited Kinetics. *Phys. Rev. Lett.* **2004**, *93*, 166101.
18. N'Diaye, A. T.; Bleikamp, S.; Feibelman, P. J.; Michely, T. Two-Dimensional Ir Cluster Lattice on a Graphene Moiré on Ir(111). *Phys. Rev. Lett.* **2006**, *97*, 215501.
19. N'Diaye, A. T.; Gerber, T.; Busse, C.; Myslivecek, J.; Coraux, J.; Michely, T. A Versatile Fabrication Method for Cluster Superlattices. *New J. Phys.* **2009**, *11*, 103045.
20. Feibelman, P. J. Rebonding Effects in Separation and Surface-Diffusion Barrier Energies of an Adatom Pair. *Phys. Rev. Lett.* **1987**, *58*, 2766–2769.
21. Stumpf, R. H-Enhanced Mobility and Defect Formation at Surfaces: H on Be(0001). *Phys. Rev. B* **1996**, *53*, R4253–R4256.
22. Horch, S.; Lorensen, H. T.; Helveg, S.; Laegsgaard, E.; Stensgaard, I.; Jacobsen, K. W.; Nørskov, J. K.; Besenbacher, F. Enhancement of Surface Self-Diffusion of Platinum Atoms by Adsorbed Hydrogen. *Nature* **1999**, *398*, 134–136.
23. Feibelman, P. J. Pinning of Graphene to Ir(111) by Flat Ir Dots. *Phys. Rev. B* **2008**, *77*, 165419.
24. Mélinon, P.; Hannour, A.; Prével, B.; Bardotti, L.; Bernstein, E.; Perez, A.; Gierak, J.; Bourhis, E.; Mailly, D. Functionalizing Surfaces with Arrays of Clusters: Role of the Defects. *J. Cryst. Growth* **2005**, *275*, 317–324.
25. Palmer, R. E.; Pratontep, S.; Boyen, H.-G. Nanostructured Surfaces from Size-Selected Clusters. *Nat. Mater.* **2003**, *2*, 443–448.
26. Donner, K.; Jakob, P. Structural Properties and Site Specific Interactions of Pt with the Graphene/Ru(0001) Moiré Overlayer. *J. Chem. Phys.* **2009**, *131*, 164701.
27. The same factor 2 is found in rate equations describing the formation of one dimer out of two monomers. See, for example, ref 53.
28. Tränkenschuh, B.; Fritsche, N.; Fuhrmann, T.; Papp, C.; Zhu, J. F.; Denecke, R.; Steinrück, H.-P. A Site-Selective *In Situ* Study of CO Adsorption and Desorption on Pt(355). *J. Chem. Phys.* **2006**, *124*, 074712.
29. Björneholm, O.; Nilsson, A.; Tillborg, H.; Bennich, P.; Sandell, A.; Hernnäs, B.; Puglia, C.; Mårtensson, N. Overlayer Structure from Adsorbate and Substrate Core Level Binding Energy Shifts: CO, CCH_3 and O on Pt(111). *Surf. Sci.* **1994**, *315*, L983–L989.
30. Wang, J. G.; Li, W. X.; Borg, M.; Gustafson, J.; Mikkelsen, A.; Pedersen, T. M.; Lundgren, E.; Weissenrieder, J.; Klikovits, J.; Schmid, M.; *et al.* One-Dimensional PtO_2 at Pt Steps: Formation and Reaction with CO. *Phys. Rev. Lett.* **2005**, *95*, 256102.
31. Note that the O 1s binding energy for step adsorption from Tränkenschuh *et al.*[28] can only be assigned to atop sites at step edges with the help of a second article by the same authors.[32]
32. Tränkenschuh, B.; Papp, C.; Fuhrmann, T.; Denecke, R.; Steinrück, H.-P. The Dissimilar Twins: A Comparative, Site-Selective *In Situ* Study of CO Adsorption and Desorption on Pt(322) and Pt(355). *Surf. Sci.* **2007**, *601*, 1108–1117.
33. Gruene, P.; Fielicke, A.; Meijer, G.; Rayner, D. M. The Adsorption of CO on Group 10 (Ni, Pd, Pt) Transition-Metal Clusters. *Phys. Chem. Chem. Phys.* **2008**, *10*, 6144–6149.
34. Lauterbach, J.; Boyle, R. W.; Schick, M.; Mitchell, W. J.; Meng, B.; Weinberg, W. H. The Adsorption of CO on Ir(111) Investigated with FT-IRAS. *Surf. Sci.* **1996**, *350*, 32–44.
35. Knudsen, J.; Feibelman, P. J.; Gerber, T.; Grånäs, E.; Schulte, K.; Stratmann, P.; Andersen, J. N.; Michely, T. Clusters Binding to the Graphene Moiré on Ir(111): X-ray Photoemission Compared to Density Functional Calculations. *Phys. Rev. B* **2012**, *85*, 035407.
36. Hammer, B.; Nielsen, O. H.; Nørskov, J. K. Structure Sensitivity in Adsorption: CO Interaction with Stepped and Reconstructed Pt Surfaces. *Catal. Lett.* **1997**, *46*, 31–35.
37. Blyholder, G. Molecular Orbital View of Chemisorbed Carbon Monoxide. *J. Phys. Chem.* **1964**, *68*, 2772–2777.
38. Föhlisch, A.; Nyberg, M.; Hasselström, J.; Karis, O.; Pettersson, L. G. M.; Nilsson, A. How Carbon Monoxide Adsorbs in Different Sites. *Phys. Rev. Lett.* **2000**, *85*, 3309–3312.
39. Föhlisch, A.; Nyberg, M.; Bennich, P.; Triguero, L.; Hasselström, J.; Karis, O.; Pettersson, L. G. M.; Nilsson, A. The Bonding of CO to Metal Surfaces. *J. Chem. Phys.* **2000**, *112*, 1946–1958.

40. Feibelman, P. J.; Hammer, B.; Nørskov, J. K.; Wagner, F.; Scheffler, M.; Stumpf, R.; Watwe, R.; Dumesic, J. The CO/Pt(111) Puzzle. *J. Phys. Chem. B* **2001**, *105*, 4018–4025.
41. Kresse, G.; Furthmüller, J. Efficiency of *Ab-Initio* Total Energy Calculations for Metals and Semiconductors Using a Plane-Wave Basis Set. *Comput. Mater. Sci.* **1996**, *6*, 15–50.
42. Kresse, G.; Furthmüller, J. Efficient Iterative Schemes for *Ab Initio* Total-Energy Calculations Using a Plane-Wave Basis Set. *Phys. Rev. B* **1996**, *54*, 11169–11186.
43. Blöchl, P. E. Projector Augmented-Wave Method. *Phys. Rev. B* **1994**, *50*, 17953–17979.
44. Kresse, G.; Joubert, D. From Ultrasoft Pseudopotentials to the Projector Augmented-Wave Method. *Phys. Rev. B* **1999**, *59*, 1758–1775.
45. Perdew, J. P.; Zunger, A. Self-Interaction Correction to Density-Functional Approximations for Many-Electron Systems. *Phys. Rev. B* **1981**, *23*, 5048–5079.
46. Ceperley, D. M.; Alder, B. J. Ground State of the Electron Gas by a Stochastic Method. *Phys. Rev. Lett.* **1980**, *45*, 566–569.
47. Butt, H.-J.; Graf, K.; Kappl, M. *Physics and Chemistry of Interfaces*; Wiley-VCH: Weinheim, Germany, 2003; Chapter 7, p 118 ff.
48. Feibelman, P. J. Onset of Three-Dimensional Ir Islands on a Graphene/Ir(111) Template. *Phys. Rev. B* **2009**, *80*, 085412.
49. Tao, F.; Dag, S.; Wang, L.-W.; Liu, Z.; Butcher, D. R.; Bluhm, H.; Salmeron, M.; Somorjai, G. A. Break-Up of Stepped Platinum Catalyst Surfaces by High CO Coverage. *Science* **2010**, *327*, 850–853.
50. Lee, J.; Cowin, J. P.; Wharton, L. He Diffraction from Clean Pt(111) and (1 × 1)H/Pt(111) Surface. *Surf. Sci.* **1983**, *130*, 1–28.
51. Steininger, H.; Lehwald, S.; Ibach, H. Adsorption of Oxygen on Pt(111). *Surf. Sci.* **1982**, *123*, 1–17.
52. Coraux, J.; N'Diaye, A. T.; Engler, M.; Busse, C.; Wall, D.; Buckanie, N.; Meyer zu Heringdorf, F.-J.; van Gastel, R.; Poelsema, B.; Michely, T. Growth of Graphene on Ir(111). *New J. Phys.* **2009**, *11*, 023006.
53. Michely, T.; Krug, J. *Islands, Mounds and Atoms: Patterns and Processes in Chrystal Growth Far from Equilibrium*; Springer-Verlag: Berlin, 2004.
54. Nyholm, R.; Andersen, J. N.; Johansson, U.; Jensen, B. N.; Lindau, I. Beamline I311 at MAX-LAB: a VUV/Soft X-ray Undulator Beamline for High Resolution Electron Spectroscopy. *Nucl. Instrum. Methods Phys. Res., Sect. A* **2001**, *467−468*, 520–524.
55. van Gastel, R.; N'Diaye, A. T.; Wall, D.; Coraux, J.; Busse, C.; Buckanie, N. M.; Meyer zu Heringdorf, F.-J.; Horn von Hoegen, M.; Michely, T.; Poelsema, B. Selecting a Single Orientation for Millimeter Sized Graphene Sheets. *Appl. Phys. Lett.* **2009**, *95*, 121901.
56. Loginova, E.; Nie, S.; Thürmer, K.; Bartelt, N. C.; McCarty, K. F. Defects of Graphene on Ir(111): Rotational Domains and Ridges. *Phys. Rev. B* **2009**, *80*, 085430.
57. Horcas, I.; Fernández, R.; Gómez-Rodríguez, J. M.; Colchero, J.; Gómez-Herrero, J.; Baro, A. M. WSXM: A Software for Scanning Probe Microscopy and a Tool for Nanotechnology. *Rev. Sci. Instrum.* **2007**, *78*, 013705.